IEEE Access
Multidisciplinary | Rapid Review | Open Access Journal

Received March 24, 2022, accepted June 12, 2022, date of publication June 20, 2022, date of current version June 23, 2022.

Digital Object Identifier 10.1109/ACCESS.2022.3184017

Design of Intelligent Reflecting Surface (IRS)-Boosted Ambient Backscatter Systems

SAHAR IDREES[1,2], (Graduate Student Member, IEEE),
XIAOLUN JIA[1], (Graduate Student Member, IEEE),
SALMAN DURRANI[1], (Senior Member, IEEE),
AND XIANGYUN ZHOU[1], (Senior Member, IEEE)
[1]School of Engineering, College of Engineering and Computer Science, Australian National University, Canberra, ACT 2601, Australia
[2]Department of Electrical Engineering, University of Engineering and Technology, Lahore 54890, Pakistan

Corresponding author: Sahar Idrees (sahar.idrees@anu.edu.au)

This work was supported by the Australian Research Council's Discovery Project Funding Scheme under Project DP170100939.

ABSTRACT Passive technologies like ambient backscatter communication (AmBC) and intelligent reflecting surface (IRS) hold enormous potential for ubiquitous connectivity of Internet of Things (IoT) devices in future wireless networks. However, despite many research efforts, AmBC has so far been unable to fulfil its potential for widespread deployment, due to the weakness of backscatter signal in the presence of strong direct-link interference from the original RF source. This limits the bit error rate (BER) and hence the transmission rate and range of AmBC systems. Meanwhile, the IRS offers new degrees of freedom in enhancing a variety of systems by transforming their propagation medium and signals. In this work, we devise a novel scheme to improve the detection performance of an AmBC system using an IRS located in its proximity. The IRS augments the backscatter signal quality at the receiver by adjusting its phase shifts to balance signal strengths, ultimately improving the performance of energy detection at the receiver. Our results clearly show that an IRS of reasonable size can considerably improve the BER performance of ambient backscatter, which is an important improvement for low power IoT systems.

INDEX TERMS Ambient backscatter communication, intelligent reflecting surface (IRS), interference cancellation, bit error rate, multiple antennas, Internet of Things (IoT).

I. INTRODUCTION

A. MOTIVATION

With the evolution and expansion of the Internet of Things (IoT), pervasive connectivity among an exceedingly large number of people and devices is inevitable. Consequently, technologies that keep power consumption and RF emissions in check are highly desirable [1]. In this regard, ambient backscatter communication (AmBC) has been envisioned as a promising technology with the potential to realize energy efficient ubiquitous connectivity among the large number of devices for the Internet of Things (IoT).

In AmBC systems, a tag or backscatter device (BD) leverages existing modulated ambient signals in its surroundings (generated from RF sources like TV towers, Wi-Fi access points or a base stations from the cellular network) to convey its own information [2], [3]. The BD modulates the backscattered signal by switching between the following two states: a backscattering state, when the BD antenna is short-circuited, and a transparent state, when the BD antenna is open-circuited [2]. These states correspond to bit '0' and bit '1'. Typically, an energy detector (ED) [4] is used at the backscatter receiver (RX) to detect the AmBC symbols, by calculating the received power levels at the RX and then mapping them to corresponding transmitted signals from the BD. Consequently, the AmBC system is energy efficient as it does not require active RF signal transmission and also spectrally efficient as it shares the spectrum of the ambient RF source.

Despite the research efforts in the area of AmBC, the reliability in terms of bit error rate (BER) of such systems is still limited. This is due to the fact that the backscatter signal suffers double fading and when it arrives at the RX, it is very weak as compared to the ambient signal from the original RF source, also known as direct-link interference (DLI). The DLI is an unknown, already modulated signal,

The associate editor coordinating the review of this manuscript and approving it for publication was Zihuai Lin.

much stronger than the information signal of interest from the BD. It has been shown that, even in line-of-sight (LOS), the DLI and the AmBC signal can combine such that the received signals corresponding to bit '0' and bit '1' differ only in phase, but have very close values in terms of power [5]. In such a scenario, the ED performs poorly and BER is high.

To improve the performance of the ED, it is imperative to strengthen the backscatter signal and also to maximize the contrast between the received powers at the ED corresponding to bit '0' and '1'. In this regard, the work in [6] created a hot-spot on the BD and a good reception spot on a RX using massive MIMO at the ambient source. The work in [7] suggested frequency shifting, which is not desirable at the low-power BD. Other methods have been proposed like training sequence design [8] or general signal processing techniques [9], [10]. The work in [11] discussed minimizing the BER of AmBC systems and proposed optimal beamforming in terms of SINR maximization and zero-forcing beamforming based solutions. However, with practical system parameter values affecting backscatter signal strength, the BER is still high for these two schemes.

Another promising technology, intelligent reflecting surface (IRS) has recently emerged and is expected to revolutionize and transform future wireless networks [12]–[16]. An IRS is an array of reconfigurable reflecting elements that can interact directly with impinging signals in a controlled manner to apply a particular set of phase-shifts, thereby controlling the direction of reflection. Thus, the coordinated design of phase shifts for a large number of IRS reflectors allows reflected signals to be received constructively (or destructively) at a receiving node [17]–[19]. This allows the IRS to mitigate the inter-user interference or improve the signal quality at some specific and localized network locations. It is noteworthy, that the IRS technology is nearly passive, as it is completely based on the scattering of the electromagnetic waves. Therefore, the IRS can improve the signal reliability and overall efficiency and coverage of the network in a cost-effective and energy-efficient manner, without the need for additional densification of the network elements and/or active antennas at the transmitters and receivers [12].

B. RELATED WORK

Due to the promising potential of IRS, its usefulness in solving key issues of existing technologies like multiple-input multiple-output (MIMO) systems, millimeter-wave (mmWave) communications, terahertz (THz) communications, UAV communication and mobile-edge computing for enhancing the performance of future wireless networks has gathered a lot of interest [12], [17], [20]–[23]. Similar to these 6G technologies, passive communication systems like backscatter communication are expected to be widely deployed in IoT technology for pervasive connectivity. As a result, there will be an increased probability of an IRS being present nearby. Therefore, it is only natural to explore the opportunities afforded by IRS-aided backscatter systems as evidenced by [24]–[31].

Some of the above cited works have considered IRS-aided monostatic backscatter systems, e.g., [24] presented performance analysis, but for a simplified system model with the direct reader-to-tag link blocked while the work in [25] proposed a channel estimation scheme for the reader-tag direct channel and reader-IRS-tag reflecting channel by controlling the IRS reflection over time. An IRS-aided bistatic backscatter system was introduced in [26], solving the transmit power minimization problem while considering multiple signal reflections at the IRS due to the coexistence of the IRS and backscatter systems.

Ambient backscatter is inherently more attractive conceptually, yet more challenging as compared to monostatic and bistatic setups, as mentioned in the previous subsection. However, IRS-aided AmBC systems have the potential to efficiently overcome these limitations, due to the ability of an IRS to strengthen the signal of interest as well as perform interference mitigation. The utility of IRS for ambient backscatter is corroborated by the recent spike in the research efforts in this area [27]–[32]. In this regard, [27] presented a scheme to improve bit error rate (BER) performance for short-range backscatter communication, by using IRS phase shifts to compensate for the multipath effect of the propagation channel but for the specific case of OFDM based ambient signals. The work in [28] proposed a joint optimization scheme to use an IRS to assist a symbiotic cognitive backscattering communication system, while the work in [32] presented a channel estimation scheme for a system in which an IRS itself performs ambient backscatter. Another work [29] used a deep reinforcement learning (DRL) based framework to optimize the AmBC detection without any knowledge of CSI. Recently some experimental works have also emerged, with [30] demonstrating experimentally that by tuning the beam and the phase-shift of the IRS, the performance of ambient backscatter systems can be improved. Specifically, a ''hot spot'' is created on the tag or ''coherent spots'' are created both on the tag and the reader, so that all the direct and IRS-reflected waves combine coherently at the reader, thereby improving performance. The work in [31] is another experimental work, that presented a prototype of an IRS and its simple voltage dependent model to optimize the phase of the scattered field and substantiated the application of IRS in assisting AmBC systems.

Previously, one of the seminal papers in IRS literature [33], presented the joint optimization of the active transmit beamforming and the passive IRS phase shifts in conventional point-to-point MISO system and and provided a semi-definite relaxation (SDR) based centralized solution and an alternating optimization (AO) based solution. However, in an IRS-aided backscatter system, the signal model and the design of IRS phase shifts becomes a lot more challenging as the coexistance of these two reflection-based systems lead to multiple reflections at the IRS being significant [26]. Recently, the work in [28] has dealt with joint optimization of the IRS with AmBC but under the special case of a symbiotic, cognitive ambient backscatter system where the

original ambient signal and the backscatter signal are both jointly decoded at the RX.

As mentioned before, it is vital to strengthen the backscatter signal and to maximize the contrast between the received energies at the ED corresponding to the two backscatter symbols, for improved performance of the ED. In this work, we study a general IRS-aided ambient backscatter scenario. We propose a novel scheme to address the fundamental aspect of improving the detection of ambient backscatter signal at the RX. We accomplish this by designing the IRS phase shifts to improve backscatter signal strength and performing eigenvector beamforming (EBF) assisted energy detection at the RX to maximize the ratio of the two received energies.

C. OUR CONTRIBUTIONS

The main contributions of this paper are as follows:

- We study the BER minimization problem in an IRS-aided AmBC system. We present the system and signal model considering two significant reflections at the IRS and formulate a general optimization problem for BER minimization. As the general problem is difficult to solve, we propose a simpler two-step approach that is computationally less intensive.
- We find the optimal value of the IRS phase shifts that maximize the received backscatter signal strength at the RX. Since this optimization problem is non-convex we use the minorization-maximization (MM) algorithm to obtain approximate solutions for the IRS phase shifts. Despite being suboptimal, the IRS phase shifts effectively boost the strength of the backscatter signal arriving at the RX.
- Our results show that the IRS phase shifts obtained from the proposed scheme effectively boost the strength of the backscatter signal at the energy detector. With a stronger backscatter signal, the eigenvector beamformer maximizing the relative difference in received energies of bit '0' and bit '1' leads to an improved BER under realistic channel parameters as compared to the previous schemes, which is an important improvement for IoT systems.

D. NOTATION AND PAPER ORGANIZATION

The following notation is used in this paper. $j = \sqrt{-1}$ denotes the complex unit, and $\mathbb{R}$ and $\mathbb{C}$ denote the set of real and complex numbers, respectively. $|\cdot|$ and $\mathrm{Re}\{\cdot\}$ denote the magnitude and the real part of a complex number, respectively. $\mathcal{CN}(\mu, \sigma^2)$ represents a complex Gaussian distribution with mean μ and variance σ^2. Vector and matrix quantities are denoted using lowercase and uppercase boldface letters, respectively, as in $\mathbf{a}$ and $\mathbf{A}$. $\mathbf{I}$ denotes the identity matrix of variable size. $\|\mathbf{a}\|$ denotes the Euclidean norm of a vector; $\mathrm{tr}(\mathbf{A})$, $\mathbf{A}^T$ and $\mathbf{A}^H$ denote the trace, transpose and the Hermitian transpose of $\mathbf{A}$, respectively. Finally, $\exp(\cdot)$ is the exponential function, $\mathrm{sgn}(\cdot)$ represents the signum function, $\log(\cdot)$ is the logarithmic function and $\mathcal{Q}(\cdot)$ is the Q-function.

The rest of the paper is organized as follows. Section II describes the system model and assumptions. Section III presents the signal model of the system in terms of mathematical equations. Section IV presents the proposed scheme and the associated optimization problems. Section V solves the optimization problem. Section VI presents and discusses the numerical results. Finally, Section VII concludes the paper.

II. SYSTEM MODEL

We consider a system in which an IRS with N passive reflecting elements is deployed to assist a BD to communicate to a RX by backscattering ambient signals from an ambient source (AS). We model the system in a three dimensional setup as shown in Fig. 1. The location coordinates of the IRS, AS, BD and the RX are $(0, 0, l_z^{\mathrm{I}})$, $(l_x^{\mathrm{A}}, l_y^{\mathrm{A}}, l_z^{\mathrm{A}})$, $(l_x^{\mathrm{B}}, l_y^{\mathrm{B}}, 0)$ and $(l_x^{\mathrm{R}}, l_y^{\mathrm{R}}, 0)$ respectively. The distance among the system components is represented by d_{i-j} and the corresponding pathloss as β_{i-j}, where i and j represent the respective components of the system. Note that for the links through the IRS, the pathloss of the two links (to and from IRS) is lumped into a single constant, e.g., $\beta_{\text{A-I-R}}$ is the pathloss associated with the AS to IRS to RX link [18].

The BD is a single-antenna device whereas the RX has M antennas. The IRS is equipped with its own power supply and a smart controller, which is connected with the RX via a separate reliable wireless link and is responsible for coordinating their operation as well as exchanging information such as reflection coefficients and channel state information (CSI). We assume perfect CSI knowledge [28] as CSI acquisition is beyond the scope of this work and should be addressed separately.[1] As the BD performs diffuse reflection, we ignore the signals reflected two or more times at the BD due to severe power loss [35]. However, for the paths in which IRS is involved, we also consider the signals that undergo two reflections at the IRS, i.e., the signal going through the AS-IRS-BD-IRS-RX link, that undergoes reflection at IRS before as well as after getting backscattered by the BD, which is a unique feature of this system. The IRS can increase overall signal strength at the RX by adjusting its phase shifts to balance the signal strengths between the AS-BD and BD-RX direct and via IRS links [26].

We assume all the channels to be quasi-static, frequency non-selective and constant in each fading block. The small-scale fading for all links is modelled as independent and identically distributed (i.i.d.) Nakagami-m fading due to its mathematical tractability [36] and because it can be used to model Rayleigh as well as Rician distributions as special cases for $m = 1$ and $m \geq 1$ [37]. This channel model allows a flexible evaluation and is commonly adopted in research works on ambient backscatter as well as on IRS [38]–[40].

[1] In practice, CSI can be estimated at the RX by adapting the channel estimation methods for the IRS systems or by using deep learning [34]. In particular for our system model, channel estimation can be carried out by turning only two nodes in our system model ON at a time and estimating the relevant channels. Thus, CSI is acquired by going pair-wise among all the nodes in the system till all of the available channels are obtained.

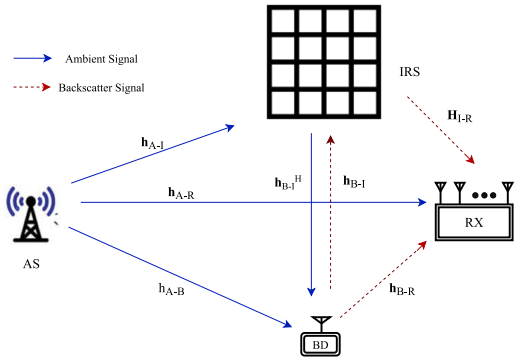

FIGURE 1. Illustration of the system model.

Let the channels from the AS, BD and RX to the IRS be represented by $\mathbf{h}_{\text{A-I}} \in \mathbb{C}^{N\times 1}$, $\mathbf{h}_{\text{B-I}} \in \mathbb{C}^{N\times 1}$ and $\mathbf{H}_{\text{R-I}} \in \mathbb{C}^{N\times M}$ respectively. Similarly, the channels from the AS to the BD and the RX are represented by $h_{\text{A-B}} \in \mathbb{C}^{1\times 1}$ and $\mathbf{h}_{\text{A-R}} \in \mathbb{C}^{M\times 1}$ respectively, while the channel from the BD to the RX is represented by $\mathbf{h}_{\text{B-R}} \in \mathbb{C}^{M\times 1}$.

III. SIGNAL MODEL

The ambient signal is independent and identically distributed at different time instants, and follows the CSCG distribution. Let s_n be the n^{th} ambient symbol that is backscattered, i.e., $s_n \sim \mathcal{CN}(0, P_s)$ where P_s is the transmit power of the AS. The signal received at the BD is a sum of the n^{th} symbol directly from the AS and its reflection from the IRS and is given by

$$r_n = \left(h_{\text{A-B}} + \mathbf{h}_{\text{B-I}}^{H}\boldsymbol{\Theta}\mathbf{h}_{\text{A-I}}\right)s_n, \tag{1}$$

where $\mathbf{h}_{\text{B-I}}$ and $\mathbf{h}_{\text{A-I}}$ are $N \times 1$ vectors and $\boldsymbol{\Theta}$ is the $N \times N$ matrix of phase shift values at the IRS such that $\boldsymbol{\Theta} = \text{diag}(e^{j\theta_1}, \cdots, e^{j\theta_N})$ and θ_n being the phase shifts of individual elements of the IRS with $\theta_n \in [0, 2\pi), \forall n$.

The BD modulates its information bits over the ambient signals by changing its antenna impedance. We adopt on--off keying at the BD, which means that the ambient signal is fully reflected when bit '1' is transmitted and there is no reflection when bit '0' is transmitted. Thus, if we denote the BD's symbol as b, we have $b \in \{0, 1\}$. Since the backscatter link is typically weaker than the direct link, the BD transmits at a much lower rate than that of the AS [11]. We assume that the BD symbol b remains unchanged for S consecutive ambient symbols. So S can be taken as the backscatter symbol length. Thus, during one BD symbol period, the backscattered signal from the BD to the RX is given by

$$x_n = \left(\sqrt{\beta_{\text{A-B}}}h_{\text{A-B}} + \sqrt{\beta_{\text{A-I-B}}}\mathbf{h}_{\text{B-I}}^{H}\boldsymbol{\Theta}\mathbf{h}_{\text{A-I}}\right)bs_n, \tag{2}$$

where s_n is the n^{th} ambient symbol. At the RX, the signal backscattered from the BD arrives by two paths i.e., directly and also after reflection from the IRS. Simultaneously, the original ambient signal from the AS reaches the RX directly as well as after suffering a reflection from the IRS. Assuming negligible synchronization errors [41], for the n^{th} ambient symbol that is backscattered, the overall signal received at the M antenna RX is,

$$\mathbf{y}_n = \mathbf{f}_{\text{A}}s_n + \mathbf{f}_{\text{B}}bs_n + \mathbf{z}_n, \tag{3}$$

where $\mathbf{y}_n$ is an $M \times 1$ vector, $\mathbf{z}_n \sim \mathcal{CN}(0, \sigma^2\mathbf{I}_M)$ is the AWGN and σ^2 is the noise power. $\mathbf{f}_{\text{A}}$ is the total effective channel experienced by the direct signal from the AS, i.e.,

$$\mathbf{f}_{\text{A}}(\boldsymbol{\Theta}) = \sqrt{\beta_{\text{A-R}}}\mathbf{h}_{\text{A-R}} + \sqrt{\beta_{\text{A-I-R}}}\mathbf{H}_{\text{I-R}}\boldsymbol{\Theta}\mathbf{h}_{\text{A-I}}, \tag{4}$$

and $\mathbf{f}_{\text{B}}$ is total effective channel (from the AS to BD to RX including the intermediate IRS reflections) experienced by the backscattered signal, i.e.,

$$\mathbf{f}_{\text{B}}(\boldsymbol{\Theta}) = \left(\sqrt{\beta_{\text{A-B}}}h_{\text{A-B}} + \sqrt{\beta_{\text{A-I-B}}}\mathbf{h}_{\text{B-I}}^{H}\boldsymbol{\Theta}\mathbf{h}_{\text{A-I}}\right) \times \left(\sqrt{\beta_{\text{B-R}}}\mathbf{h}_{\text{B-R}} + \sqrt{\beta_{\text{B-I-R}}}\mathbf{H}_{\text{I-R}}\boldsymbol{\Theta}\mathbf{h}_{\text{B-I}}\right). \tag{5}$$

Substituting (4) and (5) in (3) we get,

$$\begin{aligned}\mathbf{y}_n = \Bigg\{&\sqrt{\beta_{\text{A-R}}}\mathbf{h}_{\text{A-R}} + \sqrt{\beta_{\text{A-I-R}}}\mathbf{H}_{\text{I-R}}\boldsymbol{\Theta}\mathbf{h}_{\text{A-I}} \\ &+\Bigg(\sqrt{\beta_{\text{A-B}}\beta_{\text{B-R}}}h_{\text{A-B}}\mathbf{h}_{\text{B-R}} \\ &+\sqrt{\beta_{\text{A-B}}\beta_{\text{B-I-R}}}h_{\text{A-B}}\mathbf{H}_{\text{I-R}}\boldsymbol{\Theta}\mathbf{h}_{\text{B-I}} \\ &+\sqrt{\beta_{\text{A-I-B}}\beta_{\text{B-R}}}\mathbf{h}_{\text{B-R}}\mathbf{h}_{\mathbf{B-I}}{}^{H}\boldsymbol{\Theta}\mathbf{h}_{\text{A-I}} \\ &+\sqrt{\beta_{\text{A-I-B}}\beta_{\text{B-I-R}}}\mathbf{H}_{\text{I-R}}\boldsymbol{\Theta}\mathbf{h}_{\text{B-I}}\mathbf{h}_{\text{B-I}}^{H}\boldsymbol{\Theta}\mathbf{h}_{\text{A-I}}\Bigg)b\Bigg\}s_n + \mathbf{z}_n.\end{aligned} \tag{6}$$

The receiver performs receive beamforming on the received signal $\mathbf{y}_n$ to obtain

$$v_n = \mathbf{w}^H\mathbf{y}_n = \mathbf{w}^H(\mathbf{f}_{\text{A}}(\boldsymbol{\Theta}) + \mathbf{f}_{\text{B}}(\boldsymbol{\Theta})b)s_n + \mathbf{w}^H\mathbf{z}_n, \tag{7}$$

where $\mathbf{w}$ represents the receive beamforming vector. v_n then follows CSCG distribution such that,

$$v_n \sim \begin{cases}\mathcal{CN}(0, C_0), & \text{if } b = 0\\ \mathcal{CN}(0, C_1), & \text{if } b = 1,\end{cases} \tag{8}$$

where

$$C_0 = \mathbf{w}^H\mathbf{R}_0\mathbf{w} \tag{9}$$

$$C_1 = \mathbf{w}^H\mathbf{R}_1\mathbf{w} \tag{10}$$

are the energies received at the RX when bits 0 and 1 are transmitted respectively by the BD. Note that $\mathbf{R_0}$ and $\mathbf{R_1}$ are given by:

$$\mathbf{R}_0 = P_s\ \mathbf{f}_{\text{A}}(\boldsymbol{\Theta})\mathbf{f}_{\text{A}}(\boldsymbol{\Theta})^H + \sigma^2\mathbf{I}_M \tag{11}$$

$$\mathbf{R}_1 = P_s\ \left(\mathbf{f}_{\text{A}}(\boldsymbol{\Theta}) + \mathbf{f}_{\text{B}}(\boldsymbol{\Theta})\right)\left(\mathbf{f}_{\text{A}}(\boldsymbol{\Theta}) + \mathbf{f}_{\text{B}}(\boldsymbol{\Theta})\right)^H + \sigma^2\mathbf{I}_M. \tag{12}$$

The output v_n of the receive beamformer then goes to the energy detector that compares it against a decision threshold

T to detect whether b sent by the BD was a 0 or 1:

$$V = \frac{\epsilon}{S}\sum_{n=1}^{S}\left|\mathbf{w}^H v_n\right|^2 \gtrless_{b=0}^{b=1} T, \tag{13}$$

where $\epsilon = sgn(C_1 - C_0)$ and $T = \frac{\epsilon C_1 C_0}{C_1 - C_0}\ln\frac{C_1}{C_0}$ [11]. To evaluate the BER of the system, we define the *generalized relative channel difference (GRCD)* [11], [29] as the energy ratio between the symbol with the higher energy and the symbol with the lower energy, i.e.,

$$\Delta_C \triangleq \max\left\{\frac{C_1}{C_0}, \frac{C_0}{C_1}\right\} = \max\left\{\frac{\mathbf{w}^H\mathbf{R}_1\mathbf{w}}{\mathbf{w}^H\mathbf{R}_0\mathbf{w}}, \frac{\mathbf{w}^H\mathbf{R}_0\mathbf{w}}{\mathbf{w}^H\mathbf{R}_1\mathbf{w}}\right\} \tag{14}$$

For a reasonably large S, using the central limit theorem, the BER is given by [11], [29] as[2]

$$P_e = \frac{1}{2}\Big[\mathcal{Q}\Big(\sqrt{S}\Big(\frac{\Delta_C\log\Delta_C}{\Delta_C - 1} - 1\Big)\Big) + \mathcal{Q}\Big(\sqrt{S}\Big(1 - \frac{\log\Delta_C}{\Delta_C - 1}\Big)\Big)\Big] \tag{15}$$

Since $\Delta_c \geq 1$, $\left(\frac{\Delta_C\log\Delta_C}{\Delta_C - 1} - 1\right)$ and $\left(1 - \frac{\log\Delta_C}{\Delta_C - 1}\right)$ are both monotonically increasing functions of Δ_c in this range. Therefore, due to the monotonicity of the Q-function, the GRCD directly measures the BER.

IV. PROPOSED BEAMFORMING SCHEME

A. PROBLEM FORMULATION

We study the BER minimization problem in an IRS-aided AmBC system. To minimize the BER we use the GRCD defined in (14). The GRCD measures the ratio of the magnitudes of the energies of the two symbols received at the RX and directly determines the BER of the energy detector based AmBC system [11], [29]. To minimize the BER, we find the phase shift matrix $\mathbf{\Theta}$ and the receive beamforming vector $\mathbf{w}$ to maximize the GRCD

$$\text{(P1)}: \max_{\mathbf{\Theta},\mathbf{w}} \quad \Delta_C \tag{16a}$$
$$\text{s.t.} \quad |e^{j\theta_n}| = 1, \quad \forall n \in \{1, 2, \ldots, N\} \tag{16b}$$

(P1) is not a convex optimization problem as the objective function is non-convex with respect to $\mathbf{w}$ and $\mathbf{\Theta}$, although the constraints are convex. In general, there is no standard method for solving such non-convex problems optimally [33].

B. PROPOSED SCHEME

Instead of searching for the optimal values of $\mathbf{\Theta}$ and $\mathbf{w}$ in the entire solution space defined by constraint (16b), we note that the AmBC system has a unique characteristic of detecting a weak backscatter signal from the BD in the presence of very strong DLI. Leveraging this unique inherent characteristic of such systems, significant BER improvement can be brought about by strengthening the backscatter signal and by increasing the contrast in the received energies corresponding to bit '0' and bit '1' being sent by the BD. So instead of solving (P1), which takes into account the joint optimization of $\mathbf{\Theta}$ and $\mathbf{w}$ to maximize GRCD, we propose a two-step sub-optimal strategy and show that its performance is comparable to the optimal solution of (P1) obtained by exhaustive search.

We propose to use an IRS for the specific purpose of enhancing the quality of the backscatter signal arriving at the RX by balancing the signal strengths of the direct and reflected paths. In particular, we first find the IRS phase shifts that maximize the backscatter signal strength arriving at the RX. Afterwards, we employ optimal beamforming at the RX, which maximizes the GRCD, that depends on the ratio of received energies corresponding to bits '0' and '1'. Finally, we perform energy detection on the backscatter signal. It is noteworthy that owing to the non-convexity of the problems and the number of variables involved, alternating optimization is generally the go-to technique for problems involving optimization over multiple variables in IRS-based systems. In contrast, our proposed scheme consists of just two steps performed sequentially and is therefore computationally less intensive.

Our proposed scheme can be broken down into the following two steps:

- In the first step, as the BD sends a known signal, we find the phase shifts at the IRS to maximize the strength of the backscatter signal arriving at the RX. To this end we can write the following optimization problem:

$$\text{(P2)}: \max_{\mathbf{\Theta}} \quad ||\mathbf{f}_B(\mathbf{\Theta})||^2 \tag{17a}$$
$$\text{s.t.} \quad |e^{j\theta_n}| = 1, \quad \forall n \in \{1, 2, \ldots, N\} \tag{17b}$$

- In the second step, the IRS sets its phase shifts according to $\mathbf{\Theta}^*$ obtained in step 1, to strengthen the backscatter signal. The RX performs optimal beamforming based on SINR maximization principle. As mentioned before, for an energy detector based RX, the optimal receive beamforming vector is the one that maximizes the difference of the two energies corresponding to bits '0' and '1'. The difference of the two energies is measured by the GRCD defined in (14). Mathematically, we have the following optimization problem,

$$\text{(P3)}: \max_{\mathbf{w}} \quad \Delta_C \tag{18}$$

Since the IRS fixes its phase shifts according to $\mathbf{\Theta}^*$ in this step, (P3) is just an optimization over candidate beamforming vectors $\mathbf{w}$.

V. PROBLEM SOLUTION

A. SOLUTION TO (P2)

In this subsection, we solve (P2). To obtain a solution for $\mathbf{\Theta}$, we simplify the objective function in (16a) by splitting it into the product of a scalar term and a squared norm:

$$\|\mathbf{f}_B(\mathbf{\Theta})\|^2 = |\mathbf{f}_{B1}(\mathbf{\Theta})|^2\,\|\mathbf{f}_{B2}(\mathbf{\Theta})\|^2. \tag{19}$$

[2]The BER expression given here is for the case $C_1 \geq C_0$. The case of $C_0 > C_1$ is analogous.

$|\mathbf{f}_{\mathrm{B1}}(\boldsymbol{\Theta})|^2$ is given by,

$$\begin{aligned}|\mathbf{f}_{\mathrm{B1}}(\boldsymbol{\Theta})|^2 &= \left|\sqrt{\beta_{\mathrm{A\text{-}B}}}h_{\mathrm{A\text{-}B}} + \sqrt{\beta_{\mathrm{A\text{-}I\text{-}B}}}\mathbf{h}_{\mathrm{B\text{-}I}}^H\boldsymbol{\Theta}\mathbf{h}_{\mathrm{A\text{-}I}}\right|^2 \\ &= \beta_{\mathrm{A\text{-}I\text{-}B}}\mathbf{v}^H\boldsymbol{\Phi}_{\mathrm{A\text{-}I\text{-}B}}\boldsymbol{\Phi}_{\mathrm{A\text{-}I\text{-}B}}^H\mathbf{v} \\ &\quad + \sqrt{\beta_{\mathrm{A\text{-}B}}\beta_{\mathrm{A\text{-}I\text{-}B}}}\mathbf{v}^H\boldsymbol{\Phi}_{\mathrm{A\text{-}I\text{-}B}}h_{\mathrm{A\text{-}B}}^H \\ &\quad + \sqrt{\beta_{\mathrm{A\text{-}B}}\beta_{\mathrm{A\text{-}I\text{-}B}}}h_{\mathrm{A\text{-}B}}\boldsymbol{\Phi}_{\mathrm{A\text{-}I\text{-}B}}^H\mathbf{v} + \beta_{\mathrm{A\text{-}B}}|h_{\mathrm{A\text{-}B}}|^2,\end{aligned} \tag{20}$$

where $\boldsymbol{\Phi}_{\mathrm{A\text{-}I\text{-}B}} \triangleq \mathrm{diag}(\mathbf{h}_{\mathrm{A\text{-}I}}^H)\mathbf{h}_{\mathrm{B\text{-}I}}$ and $\mathbf{v} = \left[e^{j\theta_1}, \ldots, e^{j\theta_N}\right]^H$ such that $|v_n| = 1,\ \forall n \in \{1, \ldots, N\}$.

Let

$$\mathbf{S_1} = \begin{bmatrix} \beta_{\mathrm{A\text{-}I\text{-}B}}\boldsymbol{\Phi}_{\mathrm{A\text{-}I\text{-}B}}\boldsymbol{\Phi}_{\mathrm{A\text{-}I\text{-}B}}^H & \sqrt{\beta_{\mathrm{A\text{-}B}}\beta_{\mathrm{A\text{-}I\text{-}B}}}\boldsymbol{\Phi}_{\mathrm{A\text{-}I\text{-}B}}h_{\mathrm{A\text{-}B}} \\ \sqrt{\beta_{\mathrm{A\text{-}B}}\beta_{\mathrm{A\text{-}I\text{-}B}}}h_{\mathrm{A\text{-}B}}^*\boldsymbol{\Phi}_{\mathrm{A\text{-}I\text{-}B}}^H & 0 \end{bmatrix}, \bar{\mathbf{v}} = \begin{bmatrix}\mathbf{v}\\ 1\end{bmatrix}. \tag{21}$$

Then (20) can be re-written in matrix form as

$$|\mathbf{f}_{\mathrm{B1}}(\boldsymbol{\Theta})|^2 = \bar{\mathbf{v}}^H\mathbf{S}_1\bar{\mathbf{v}} + \beta_{\mathrm{A\text{-}B}}|h_{\mathrm{A\text{-}B}}|^2. \tag{22}$$

Similarly, $\|\mathbf{f}_{\mathrm{B2}}(\boldsymbol{\Theta})\|^2$ is given by,

$$\begin{aligned}\|\mathbf{f}_{\mathrm{B2}}(\boldsymbol{\Theta})\|^2 &= \left\|\sqrt{\beta_{\mathrm{B\text{-}R}}}\mathbf{h}_{\mathrm{B\text{-}R}} + \sqrt{\beta_{\mathrm{B\text{-}I\text{-}R}}}\mathbf{H}_{\mathrm{I\text{-}R}}\boldsymbol{\Theta}\mathbf{h}_{\mathrm{B\text{-}I}}\right\|^2 \\ &= \beta_{\mathrm{B\text{-}I\text{-}R}}\mathbf{v}^H\boldsymbol{\Phi}_{\mathrm{B\text{-}I\text{-}R}}\boldsymbol{\Phi}_{\mathrm{B\text{-}I\text{-}R}}^H\mathbf{v} \\ &\quad + \sqrt{\beta_{\mathrm{B\text{-}R}}\beta_{\mathrm{B\text{-}I\text{-}R}}}\mathbf{v}^H\boldsymbol{\Phi}_{\mathrm{B\text{-}I\text{-}R}}\mathbf{h}_{\mathrm{B\text{-}R}} \\ &\quad + \sqrt{\beta_{\mathrm{B\text{-}R}}\beta_{\mathrm{B\text{-}I\text{-}R}}}\mathbf{h}_{\mathrm{B\text{-}R}}^H\boldsymbol{\Phi}_{\mathrm{B\text{-}I\text{-}R}}^H\mathbf{v} + \beta_{\mathrm{B\text{-}R}}|\mathbf{h}_{\mathrm{B\text{-}R}}|^2,\end{aligned} \tag{23}$$

with $\boldsymbol{\Phi}_{\mathrm{B\text{-}I\text{-}R}} \triangleq \mathrm{diag}(\mathbf{h}_{\mathrm{B\text{-}I}}^H)\mathbf{H}_{\mathrm{I\text{-}R}}^H$ and $\mathbf{v}$ as defined above.

Again, let

$$\mathbf{S_2} = \begin{bmatrix} \beta_{\mathrm{B\text{-}I\text{-}R}}\boldsymbol{\Phi}_{\mathrm{B\text{-}I\text{-}R}}\boldsymbol{\Phi}_{\mathrm{B\text{-}I\text{-}R}}^H & \sqrt{\beta_{\mathrm{B\text{-}R}}\beta_{\mathrm{B\text{-}I\text{-}R}}}\boldsymbol{\Phi}_{\mathrm{B\text{-}I\text{-}R}}\boldsymbol{h}_{\mathrm{B\text{-}R}} \\ \sqrt{\beta_{\mathrm{B\text{-}R}}\beta_{\mathrm{B\text{-}I\text{-}R}}}\mathbf{h}_{\mathrm{B\text{-}R}}^H\boldsymbol{\Phi}_{\mathrm{B\text{-}I\text{-}R}}^H & 0 \end{bmatrix}. \bar{\mathbf{v}} = \begin{bmatrix}\mathbf{v}\\ 1\end{bmatrix}. \tag{24}$$

Then (23) can also be re-written in matrix form as follows:

$$|\mathbf{f}_{\mathrm{B2}}(\boldsymbol{\Theta})|^2 = \bar{\mathbf{v}}^H\mathbf{S}_2\bar{\mathbf{v}} + \beta_{\mathrm{B\text{-}R}}|\mathbf{h}_{\mathrm{B\text{-}R}}|^2, \tag{25}$$

Substituting (22) and (25) in (19). we get,

$$G_o(\bar{\mathbf{v}}) = \bar{\mathbf{v}}^H\mathbf{S}_2\bar{\mathbf{v}}\bar{\mathbf{v}}^H\mathbf{S}_1\bar{\mathbf{v}} + k_1\bar{\mathbf{v}}^H\mathbf{S}_2\bar{\mathbf{v}} + k_2\bar{\mathbf{v}}^H\mathbf{S}_1\bar{\mathbf{v}} + k_1k_2, \tag{26}$$

with $k_1 = |h_{A-B}|^2$ and $k_2 = \|\mathbf{h}_{B-R}\|^2$.

Using (26), (P2) can be written as

$$\begin{aligned}3(\mathrm{P4}):\ &\max_{\bar{\mathbf{v}}} \quad G_o(\bar{\mathbf{v}}) && \text{(27a)}\\ &\text{s.t.} \quad |\bar{\mathbf{v}}_n| = 1, \forall n \in \{1, 2, \ldots, N\} && \text{(27b)}\end{aligned}$$

In the equivalent problem (P4), the objective function (27a) is a quartic polynomial in $\bar{\mathbf{v}}$. We let $\mathbf{V} = \bar{\mathbf{v}}\bar{\mathbf{v}}^H$ so that the objective function can be expressed as a function of $\mathbf{V}$ in terms of trace (i.e., $\mathrm{tr}(\mathbf{SV})$), which is rank-one. However, since $\mathbf{S}_1$ and $\mathbf{S}_2$ are not positive semi-definite in general, one of the resulting trace terms in (27a), i.e., $\mathrm{tr}(\mathbf{S}_2\mathbf{V}\mathbf{S}_1\mathbf{V})$, turns out to be generally non-convex. Moreover, optimizing multivariate polynomials of higher degrees is an NP-hard problem [42]. Therefore, a closed-form, optimal solution is generally not available. To solve this issue, we employ the MM algorithm [26]. The MM algorithm attempts to solve this difficult problem by constructing a series of more tractable approximate sub-problems, using a convex approximation to the original objective function.

The MM algorithm leverages a surrogate function that serves as a minorizer to an objective function $f(\mathbf{x}) : \mathbb{C}^N \to \mathbb{R}$ with bounded curvature by taking the second-order Taylor expansion [43, Lemma 12]:

$$f(\mathbf{x}) \geq f(\mathbf{x}_0) + \mathrm{Re}\left\{\nabla f(\mathbf{x}_0)^H(\mathbf{x} - \mathbf{x}_0)\right\} - \frac{\ell}{2}\|\mathbf{x} - \mathbf{x}_0\|^2, \tag{28}$$

where $\mathbf{x}_0 \in \mathbb{C}^N$ is the point where the original and the surrogate functions intersect, ∇ is the gradient operator and ℓ is the maximum curvature of $f(\mathbf{x})$. According to (28), we find the minorizer $G_{m_1}(\bar{\mathbf{v}})$ to the objective function $G_o(\bar{\mathbf{v}})$ i.e.,

$$G_o(\bar{\mathbf{v}}) \geq G_m(\bar{\mathbf{v}}), \tag{29}$$

such that

$$\begin{aligned}G_{m_1}(\bar{\mathbf{v}}) = G_o(\bar{\mathbf{v}_0}) + \bar{\mathbf{v}}_0^H\mathbf{U}(\bar{\mathbf{v}} - \bar{\mathbf{v}}_0) + (\bar{\mathbf{v}} - \bar{\mathbf{v}}_0)^H\mathbf{U}\bar{\mathbf{v}}_0 \\ - \frac{\ell}{2}\|\bar{\mathbf{v}} - \bar{\mathbf{v}}_0\|^2,\end{aligned} \tag{30}$$

with $\mathbf{U} = \mathbf{S}_1\bar{\mathbf{v}}_0\bar{\mathbf{v}}_0^H\mathbf{S}_2 + \mathbf{S}_2\bar{\mathbf{v}}_0\bar{\mathbf{v}}_0^H\mathbf{S}_1 + k_2\mathbf{S}_1 + k_1\mathbf{S}_2$ being a Hermitian matrix obtained from the derivative of $G_o(\bar{\mathbf{v}}_0)$. Expanding (30) we get,

$$\begin{aligned}G_{m_1}(\bar{\mathbf{v}}) = -\frac{\ell}{2}\Bigg(\bar{\mathbf{v}}^H\mathbf{I}\bar{\mathbf{v}} + \bar{\mathbf{v}}^H\left(-\frac{2}{\ell}\mathbf{U}\bar{\mathbf{v}}_0 - \mathbf{I}\bar{\mathbf{v}}_0\right) \\ + \left(-\frac{2}{\ell}\mathbf{U}\bar{\mathbf{v}}_0 - \mathbf{I}\bar{\mathbf{v}}_0\right)^H\bar{\mathbf{v}}\Bigg) + k,\end{aligned} \tag{31}$$

where k denotes the cumulative sum of all constant terms. (31) is of quadratic form, and can be rewritten as:

$$G_{m_1}(\bar{\bar{\mathbf{v}}}) = \bar{\bar{\mathbf{v}}}^H\mathbf{Q}\bar{\bar{\mathbf{v}}} + k \tag{32}$$

where

$$\mathbf{Q} = -\begin{bmatrix} \mathbf{I} & -\frac{2}{\ell}\mathbf{U}\bar{\mathbf{v}}_0 - \mathbf{I}\bar{\mathbf{v}}_0 \\ (-\frac{2}{\ell}\mathbf{U}\bar{\mathbf{v}}_0 - \mathbf{I}\bar{\mathbf{v}}_0)^H & 0 \end{bmatrix}, \bar{\bar{\mathbf{v}}} = \begin{bmatrix}\bar{\mathbf{v}}\\ 1\end{bmatrix}. \tag{33}$$

Letting $\bar{\bar{\mathbf{V}}} = \bar{\bar{\mathbf{v}}}\bar{\bar{\mathbf{v}}}^H$, a transformed version of Problem (P4) is given by

$$\begin{aligned}(\mathrm{P5}):\ &\max_{\bar{\bar{\mathbf{V}}}} \quad \mathrm{tr}(\mathbf{Q}\bar{\bar{\mathbf{V}}}) + k, && \text{(34a)}\\ &\text{s.t.} \quad \bar{\bar{\mathbf{V}}}_{n,n} = 1, \quad \forall n \in \{1, \ldots, N+2\}, && \text{(34b)}\\ &\qquad \bar{\bar{\mathbf{V}}} \succeq 0, && \text{(34c)}\\ &\qquad \mathrm{rank}(\bar{\bar{\mathbf{V}}}) = 1. && \text{(34d)}\end{aligned}$$

One potential strategy to tackle this situation is to drop the rank-one constraint, such that Problem (P5) becomes a convex semidefinite program (SDP), which is solvable using CVX [44]. The solution obtained by CVX may or may not be rank one. Therefore, Gaussian randomization [45] can be used, yielding a candidate vector, whose last element is dropped and then the resulting $N \times 1$ vector is substituted in (31) during the next MM iteration to obtain a new approximation to $G_o(\bar{\mathbf{v}})$. This process needs to be repeated till the MM algorithm converges.

The above stated process incurs a formidable complexity of the order of $O(I(N+2)^{4.5})$, where I is the number MM iterations, and the $(N+2)^{4.5}$ is the SDP complexity [46]. An alternative, less costly approach is to further take a minorizer G_{m_2} to G_{m_1}, similar to the procedure in [47] such that,

$$G_o(\bar{\mathbf{v}}) \geq G_{m_1}(\bar{\bar{\mathbf{v}}}) \geq G_{m_2}(\bar{\bar{\mathbf{v}}}). \tag{35}$$

where

$$G_{m_2}(\bar{\bar{\mathbf{v}}}) = \bar{\bar{\mathbf{v}}}^H \mathbf{T} \bar{\bar{\mathbf{v}}} + 2\mathrm{Re}\{\bar{\bar{\mathbf{v}}}^H (\mathbf{Q}-\mathbf{T})\bar{\bar{\mathbf{v}}}_0\} + \bar{\bar{\mathbf{v}}}_0{}^H (\mathbf{Q}-\mathbf{T})\bar{\bar{\mathbf{v}}}_0 \tag{36}$$

Note that $\mathbf{T} = \lambda^{-}\mathbf{I}$, where λ^{-} is the minimum eigenvalue of $\mathbf{Q}$ and $\bar{\bar{\mathbf{v}}}_0$ is as before. G_{m_2} can serve as the objective function in each MM iteration instead of G_{m_1}. Ignoring the constant terms, the sub-problem to be solved in each iteration of the MM algorithm reduces to:

$$\begin{aligned}
(\text{P6}): \quad & \max_{\bar{\bar{\mathbf{v}}}} \quad 2\mathrm{Re}\{\bar{\bar{\mathbf{v}}}^H (\mathbf{Q}-\mathbf{T})\bar{\bar{\mathbf{v}}}_0\}, && \text{(37a)}\\
& \text{s.t.} \quad |\bar{\bar{\mathbf{v}}}_{n,n}| = 1, \quad \forall n \in \{1,\ldots,N+2\}, && \text{(37b)}\\
& \qquad \bar{\bar{\mathbf{v}}}_{j,j} = 1, j = \{N+1, N+2\}, && \text{(37c)}
\end{aligned}$$

The closed form solution to (P6) is given by $\bar{\bar{\mathbf{v}}}^* = e^{j\arg((\mathbf{Q}-\mathbf{T})\bar{\bar{\mathbf{v}}}_0)}$.

It is noteworthy that the objective function G_o in the original problem (P4) is bounded from above, as $\mathbf{S}_1$ and $\mathbf{S}_2$ are constant matrices and $\|\bar{\mathbf{v}}\|^2 = N$ is a finite constant. Moreover, G_{m_1} and G_{m_2} can each serve as a minorizer to G_o and can also can be shown to satisfy the conditions for the convergence of MM algorithm, as stated in [43], [47]. We run the MM algorithm with G_{m_2} as the surrogate function, such that a closed form optimal solution in terms of $\bar{\bar{\mathbf{v}}}$ is returned in each iteration. Therefore, the solution obtained in each subsequent iteration of the MM algorithm will result in a monotonic increase in G_o and will ultimately converge to a local optimum. This approach, summarized in **Algorithm 1**, will incur a complexity of the order of $O(IN)$.

B. SOLUTION TO (P3)

Similarly to [11], (P3) is solved as follows: Substituting the definition of GRCD from (14) into (18) we get:

$$(\text{P3}): \quad \max_{\mathbf{w}} \left(\max \left(\frac{\mathbf{w}^{\mathrm{H}}\mathbf{R}_0\mathbf{w}}{\mathbf{w}^{\mathrm{H}}\mathbf{R}_1\mathbf{w}}, \frac{\mathbf{w}^{\mathrm{H}}\mathbf{R}_1\mathbf{w}}{\mathbf{w}^{\mathrm{H}}\mathbf{R}_0\mathbf{w}} \right) \right). \tag{38}$$

Algorithm 1 MM Algorithm for Solving (P4)

1: **Initialize:** Random IRS phase shifts $\boldsymbol{\theta}$; set iteration number $i = 1$.
2: Obtain $\bar{\mathbf{v}}$ from $\boldsymbol{\theta}$ and set $\bar{\mathbf{v}}_0^{(i)} = \bar{\mathbf{v}}$.
3: **while** the rate of change in objective function (26) is above a threshold $\varepsilon > 0$ **do**
do
4: Construct $\mathbf{Q}$ from $\bar{\mathbf{v}}_0^{(i)}$ and $\mathbf{U}$.
5: Set $\bar{\mathbf{v}}^{(i+1)} \leftarrow \bar{\bar{\mathbf{v}}}^* = e^{j\arg((\mathbf{Q}-\mathbf{T})\bar{\bar{\mathbf{v}}}_0)}$ for next iteration.
6: Update iteration number $i \leftarrow i+1$.
7: **end while**
8: **Return:** Optimized phase shift vector $\mathbf{v}^*$ by dropping the last element of $\bar{\mathbf{v}}_0$ at convergence.

To solve (P3), without loss of generality we consider $f(\mathbf{w}) = \frac{\mathbf{w}^{\mathrm{H}}\mathbf{R}_1\mathbf{w}}{\mathbf{w}^{\mathrm{H}}\mathbf{R}_0\mathbf{w}}$. Then to find the maximum of (P3), we differentiate $f(\mathbf{w})$ with respect to $\mathbf{w}$ and set it equal to zero, i.e.,

$$\frac{d}{d\mathbf{w}} f(\mathbf{w}) = \frac{2\mathbf{R}_1\mathbf{w}\left(\mathbf{w}^{\mathrm{H}}\mathbf{R}_0\mathbf{w}\right) - 2\mathbf{R}_0\mathbf{w}\left(\mathbf{w}^{\mathrm{H}}\mathbf{R}_1\mathbf{w}\right)}{\left(\mathbf{w}^{\mathrm{H}}\mathbf{R}_0\mathbf{w}\right)^2} = 0. \tag{39}$$

Rearringing (39) we obtain $\mathbf{R}_1\mathbf{w} = f(\mathbf{w})\,\mathbf{R}_0\mathbf{w}$, which can be recognized as a generalized eigenvalue problem with $\lambda = f(\mathbf{w})$ being the eigenvalue and $\mathbf{w}$ the corresponding eigenvector. Let $\lambda_{\max}$ and $\lambda_{\min}$ be the maximum and minimum generalized eigenvalues, and $\mathbf{w}_{\max}$ and $\mathbf{w}_{\min}$ be the corresponding eigenvectors, respectively. Then, the optimal beamforming vector is by $\mathbf{w}_{\max}$ if $\lambda_{\max} \geq \frac{1}{\lambda_{\min}}$ and it is $\mathbf{w}_{\min}$ otherwise.

VI. RESULTS

In this section, we provide simulation results to evaluate our proposed scheme. We consider an ambient backscatter scenario, with an ambient signal of frequency 915 MHz. The AS, BD, IRS and RX are located at $[-50, 2, 5]$, $[10, 2, 0]$, $[0, 0, 2]$ and $[15, 2, 0]$ respectively, with all the coordinates in meters. The values of rest of system parameters are: $\alpha = 2.5$, $G_s = 1.5$ dB, $G_r = 1.5$ dB, $P_s = 30$ dBm, $\sigma^2 = -80$ dBm. The Nakagami-m parameter is set to 5 for all the links among IRS, BD and RX, while it is set to 1 for the links from IRS, BD and RX to the AS [38]–[40]. We set the backscatter frame consisting of 100 backscatter symbols and average our results over 1.5×10^6 Monte-Carlo runs.

For the purpose of comparison with our proposed scheme for the IRS-aided system, the alternating optimization based successive refinement of IRS phase shifts presented in [33] can be adapted as a benchmark. However, this adaptation is not straightforward as it does not yield a meaningful bound, unless some form of strengthening the backscatter signal or DLI cancellation is included. So we resort to exhaustive search to solve (P1) and establish a benchmark for IRS-aided AmBC system. In addition we also present the following benchmarks for comparison:

- IRS-less system with zero-forcing beamforming (ZFBF) at the RX.

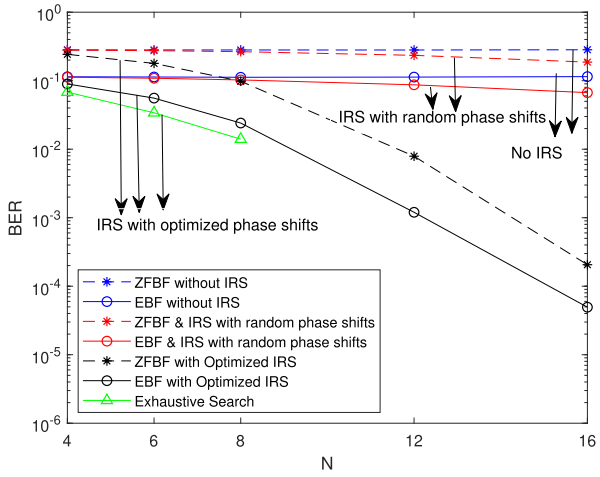

FIGURE 2. BER versus N with $P_s = 30$ dBm, $S = 60$, $M = 4$ with IRS located at $(12, 2, 5)$.

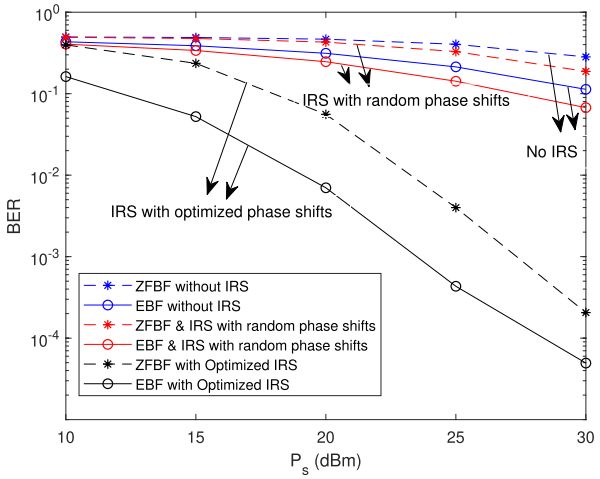

FIGURE 3. BER versus P_s with $S = 60$, $N = 16$, $M = 4$ with IRS located at $(12, 2, 5)$.

- IRS-less system with eigenvector beamforming (EBF) at the RX.
- IRS-aided system with ZFBF at the RX and IRS phase shifts set to random values.
- IRS-aided system with EBF at the RX and IRS phase shifts set to random values.
- IRS-aided system with ZFBF at the RX and IRS phase shifts calculated by solving (P2) given in (17).

Fig. 2 illustrates the BER performance of the proposed scheme with respect to the number of elements N of the IRS for $P_s = 30$ dBm and $S = 60$. The plot for exhaustive search results has only three data points highlighted by Δ for $N \in \{4, 6, 8\}$. Further data points could not be obtained because the exhaustive search method demands excessive computational resources. The plots of other five benchmarks enumerated above have also been included.

We can see that the gap between the plots for our proposed scheme and for the exhaustive search reduces as N increases. This highlights the usefulness of our scheme, as it is computationally less intensive and performs fairly closely (as N increases) to the results obtained by solving (P1) by exhaustive search.

Comparing the results of the proposed scheme with the benchmarks we can see that the performance of the system without the IRS is worst, regardless of the beamforming used at the RX. For the systems including an IRS with random phase shifts, we see a marginal improvement over the baseline schemes. However, with an optimized IRS, there is a marked improvement in the performance of both eigenvector and zero-forcing beamforming based energy detection. In all scenarios, EBF at the RX performs better than its zero-forcing counterpart, because the ZFBF removes the direct-link interference altogether and reduces overall signal strength at the RX, leading to performance loss. On the other hand, EBF at the RX achieves the perfect balance by maximizing the contrast between the two received energies and when employed with an optimized IRS for maximizing backscatter signal strength, best performance is achieved.

It is also clear from Fig. 2 that the BER significantly decreases with the increase of the IRS size. Even with an IRS of modest size $N = 4$, the BER is 8.9×10^{-2}. For an IRS of size $N = 16$ the BER drops to as low as 4.94×10^{-5}. We can see that with increase in its size, the IRS is more effective in balancing the signal strengths to increase the strength of received backscatter signal at the RX and thus reducing the BER further. Thus, an IRS of reasonable size can effectively boost the backscatter signal and thereby assist the RX in reducing the BER of energy detection.

Fig. 3 illustrates the BER performance with varying P_s, i.e., transmit power of the AS, for $N = 16$ and $S = 60$. It is seen that the BER of our proposed detector significantly decreases with the increase of P_s. This is in contrast to conventional AmBC using simple energy detection at the RX [48], wherein, the BER did not decrease much with the increase of ambient signal power, but levels off in the high SNR region. This is due to the fact that the backscatter signal is inherently very weak. So when P_s increases, the subsequent increase in the DLI is orders of magnitude stronger than in the backscatter signal. Consequently, the BER does not decrease much. To solve this issue, in benchmarks 1 and 2 originally proposed in [11], use ZFBF to remove DLI and EBF to maximize energy difference between the two backscatter symbols respectively, prior to energy detection at the RX. However, with practical system values, the backscatter signal is still very weak. Consequently, the relative energy difference between the signals corresponding to bit '1' and bit '0' received at the ED is very low, which leads to poor energy detection and the BER is still high. However, with the introduction of IRS, even with random phase shifts (benchmarks 3 and 4), the BER performance is somewhat improved. Finally, with an IRS optimized for maximizing backscatter signal strength, the BER performance drastically improves with increase in P_s as indicated by the steepness of

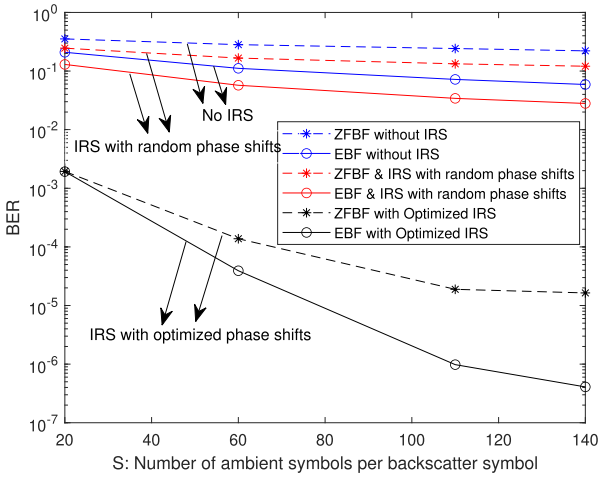

FIGURE 4. R versus S with $P_s = 30$ dBm, $N = 16$, $M = 4$ with IRS located at (12, 2, 5).

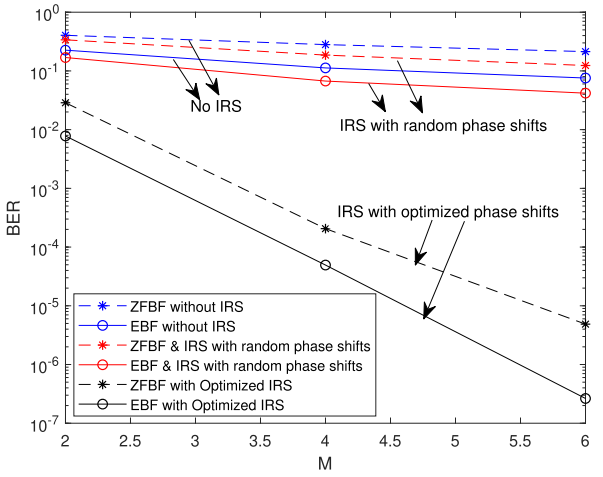

FIGURE 5. BER versus M with $P_s = 30$ dBm, $S = 60$, $N = 16$ with IRS located at (12, 2, 5).

the curve for our proposed scheme as well as for the ZFBF based solution.

Fig. 4 illustrates the BER of our scheme for different values of S, i.e., the number of ambient symbols for which the backscatter symbol transmitted remains the same. For this plot, $P_s = 30$ dBm and $N = 16$. It is clear from the figure, that the performance in terms of BER of our proposed scheme as well as all benchmarks improves with an increase in S, at the cost of a lower transmission rate. Even with a low value of $S = 20$ (corresponding to a higher transmission rate at the BD) the BER is 1.1×10^{-3}. It is also observed that as S increases, the slope of the BER curve somewhat tapers off. This is an encouraging outcome meaning that there is no significant advantage in extending the backscatter symbol lengths beyond a certain value as the IRS guarantees some performance improvement regardless of the backscatter transmission parameters.

Fig. 5 illustrates the performance of our scheme for values of number of receive antennas M with $N = 16$, $P_s = 30$ dBm and $S = 60$. It can be seen that the performance improves for all bechmarks with the increase of M, due to the increased capability of beamforming at the RX. However, it is noteworthy, that for our proposed scheme, i.e., optimized IRS with EBF at the RX and the benchmark scheme with optimized IRS and ZFBF at the RX, the descent of the BER curves is significantly steeper than in the other benchmarks. This shows that with an optimized IRS assisting the backscatter signal, the EBF at the RX can more efficiently separate the powers corresponding to the two backscatter symbols, resulting in much improved BER.

A plot of BER for three different placements of the IRS is shown in Fig. 6. We maintain the y and z coordinates of the IRS and move it parallel to the x-axis. Considering that we have kept the AS, BD and RX in a straight line in the $x-y$ plane, the three values of BER are obtained as we move the IRS from (8, 2, 5) (between AS and BD) to (12, 2, 5) (between BD and RX) to (18, 2, 5) (on the other side of RX,

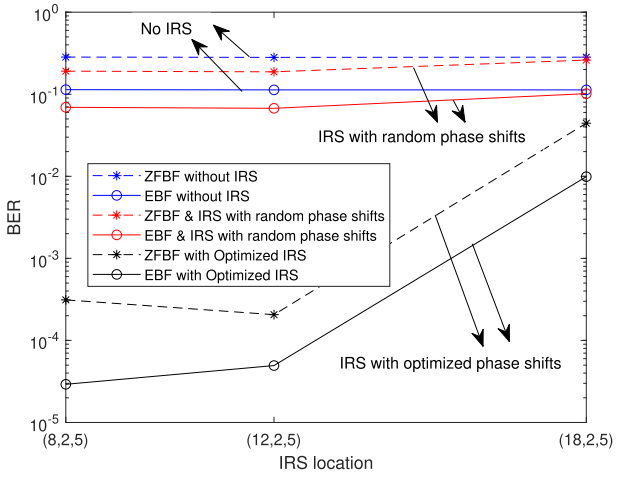

FIGURE 6. BER versus IRS position with $P_s = 30$ dBm, $S = 60$, $N = 16$ and $M = 4$.

away from AS and BD). We can see that as the IRS is moved to the other side of the RX i.e., to (18, 2, 5), the BER goes up for all the schemes, as the increased distance of the IRS from the BD and the AS results in weakening the backscatter signal arriving at the RX. However, it is interesting to note that as the IRS moves from (8, 2, 5) to (12, 2, 5), the BER goes down for the ZFBF with optimized IRS benchmark, whereas it increases for our proposed scheme EBF with optimized IRS. This is due to the fact that the ZFBF at the RX completely eliminates the direct-link signal from the AS. Therefore, the IRS located at (12, 2, 5) enjoys shorter distances to the BD and the RX and yields a smaller BER. On the other hand, our proposed scheme optimizes the received signal strength over the IRS reflection pattern and receive beamforming at the RX by maximizing the GRCD defined in (14). Therefore, when the IRS is at (8, 2, 5), it is closer to the AS as well as the BD, while the distance from the RX is greater, but still reasonable. Therefore, the IRS is more effective is enhancing the signal strength and hence the GRCD, resulting in a lower BER at

(8, 2, 5). The BER increases as we move further away from the AS. Thus, we can conclude that for our proposed scheme, the IRS needs to be positioned such that it is as close to the AS as possible, while maintaining a short distance from the BD and the RX.

VII. CONCLUSION

In this work, an IRS aided AmBC system was studied and a new scheme was devised to im42‘xprove its performance in terms of BER. The non-convex problem of optimizing the phase shifts at the IRS for maximizing the backscatter signal strength arriving at the RX was addressed using SDR within MM algorithm. Our findings showed that with an IRS of moderate size enhancing the AmBC system, the BER performance is significantly improved. The reduced BER can be instrumental in increasing the rate and range of AmBC systems. The scheme proposed in this paper can be extended to multiple backscatter devices, where the role of IRS in aiding in collision avoidance can be studied as well. Moreover, future work can include the CSI estimation problem of an IRS assisted ambient backscatter system.

ACKNOWLEDGMENT

This research/project also took assistance of resources and services from the National Computational Infrastructure (NCI), which is supported by the Australian Government.

REFERENCES

[1] A. Gati, F. E. Salem, A. M. G. Serrano, D. Marquet, S. Le Masson, T. Rivera, D.-T. Phan-Huy, Z. Altman, J.-B. Landre, O. Simon, E. Le Rouzic, F. Bourgart, S. Gosselin, M. Vautier, E. Gourdin, T. En-Najjary, M. El-Tabach, R.-M. Indre, G. Gerard, and G. Delsart, "Key technologies to accelerate the ICT green evolution—An operator's point of view," 2019, *arXiv:1903.09627*.

[2] V. Liu, A. Parks, V. Talla, S. Gollakota, D. Wetherall, and J. R. Smith, "Ambient backscatter: Wireless communication out of thin air," *ACM SIGCOMM Comput. Commun. Rev.*, vol. 43, no. 4, pp. 39–50, Oct. 2013.

[3] N. Van Huynh, D. T. Hoang, X. Lu, D. Niyato, P. Wang, and D. I. Kim, "Ambient backscatter communications: A contemporary survey," *IEEE Commun. Surveys Tuts.*, vol. 20, no. 4, pp. 2889–2922, 4th Quart., 2018.

[4] J. Qian, F. Gao, G. Wang, S. Jin, and H. Zhu, "Noncoherent detections for ambient backscatter system," *IEEE Trans. Wireless Commun.*, vol. 16, no. 3, pp. 1412–1422, Mar. 2017.

[5] K. Rachedi, D.-T. Phan-Huy, N. Selmene, A. Ourir, M. Gautier, A. Gati, A. Galindo-Serrano, R. Fara, and J. de Rosny, "Demo abstract: Real-time ambient backscatter demonstration," in *Proc. IEEE Conf. Comput. Commun. Workshops (INFOCOM WKSHPS)*, Apr. 2019, pp. 987–988.

[6] R. Fara, D.-T. Phan-Huy, and M. D. Renzo, "Ambient backscatters-friendly 5G networks: Creating hot spots for tags and good spots for readers," in *Proc. IEEE Wireless Commun. Netw. Conf. (WCNC)*, May 2020, pp. 1–7.

[7] D. Bharadia, K. R. Joshi, M. Kotaru, and S. Katti, "BackFi: High throughput Wi-Fi backscatter," *ACM SIGCOMM Comput. Commun. Rev.*, vol. 45, no. 4, pp. 283–296, Aug. 2015.

[8] S. Idrees, X. Zhou, S. Durrani, and D. Niyato, "Design of ambient backscatter training for wireless power transfer," *IEEE Trans. Wireless Commun.*, vol. 19, no. 10, pp. 6316–6330, Oct. 2020.

[9] G. Yang, Y.-C. Liang, R. Zhang, and Y. Pei, "Modulation in the air: Backscatter communication over ambient OFDM carrier," *IEEE Trans. Commun.*, vol. 66, no. 3, pp. 1219–1233, Mar. 2018.

[10] B. Kellogg, "Passive Wi-Fi: Bringing low power to Wi-Fi transmissions," in *Proc. 13th USENIX Symp. Netw. Syst. Design Implement.*, Mar. 2016, pp. 151–164.

[11] H. Guo, Q. Zhang, S. Xiao, and Y. Liang, "Exploiting multiple atennas for cognitive ambient backscatter communication," *IEEE Internet Things J.*, vol. 6, no. 1, pp. 765–775, Feb. 2019.

[12] M. Di Renzo, A. Zappone, M. Debbah, M.-S. Alouini, C. Yuen, J. de Rosny, and S. Tretyakov, "Smart radio environments empowered by reconfigurable intelligent surfaces: How it works, state of research, and the road ahead," *IEEE J. Sel. Areas Commun.*, vol. 38, no. 11, pp. 2450–2525, Jul. 2020.

[13] S. Gong, X. Lu, D. T. Hoang, D. Niyato, L. Shu, D. I. Kim, and Y.-C. Liang, "Toward smart wireless communications via intelligent reflecting surfaces: A contemporary survey," *IEEE Commun. Surveys Tuts.*, vol. 22, no. 4, pp. 2283–2314, Jun. 2020.

[14] Q. Wu and R. Zhang, "Towards smart and reconfigurable environment: Intelligent reflecting surface aided wireless network," *IEEE Commun. Mag.*, vol. 58, no. 1, pp. 106–112, Nov. 2020.

[15] M. A. El Mossallamy, H. Zhang, L. Song, K. G. Seddik, Z. Han, and G. Y. Li, "Reconfigurable intelligent surfaces for wireless communications: Principles, challenges, and opportunities," *IEEE Trans. Cogn. Commun. Netw.*, vol. 6, no. 3, pp. 990–1002, Sep. 2020.

[16] Y. Liu, X. Liu, X. Mu, T. Hou, J. Xu, M. Di Renzo, and N. Al-Dhahir, "Reconfigurable intelligent surfaces: Principles and opportunities," *IEEE Commun. Surveys Tuts.*, vol. 23, no. 3, pp. 1546–1577, 3rd Quart., 2021.

[17] Q. Wu, S. Zhang, B. Zheng, C. You, and R. Zhang, "Intelligent reflecting surface-aided wireless communications: A tutorial," *IEEE Trans. Commun.*, vol. 69, no. 5, pp. 3313–3351, May 2021.

[18] O. Özdogan, E. Björnson, and E. G. Larsson, "Intelligent reflecting surfaces: Physics, propagation, and pathloss modeling," *IEEE Wireless Commun. Lett.*, vol. 9, no. 5, pp. 581–585, May 2020.

[19] R. Alghamdi, R. Alhadrami, D. Alhothali, H. Almorad, A. Faisal, S. Helal, R. Shalabi, R. Asfour, N. Hammad, A. Shams, N. Saeed, H. Dahrouj, T. Y. Al-Naffouri, and M.-S. Alouini, "Intelligent surfaces for 6G wireless networks: A survey of optimization and performance analysis techniques," *IEEE Access*, vol. 8, pp. 202795–202818, 2020.

[20] P. Wang, J. Fang, X. Yuan, Z. Chen, and H. Li, "Intelligent reflecting surface-assisted millimeter wave communications: Joint active and passive precoding design," *IEEE Trans. Veh. Technol.*, vol. 69, no. 12, pp. 14960–14973, Oct. 2020.

[21] Z. Chen, X. Ma, C. Han, and Q. Wen, "Towards intelligent reflecting surface empowered 6G terahertz communications: A survey," *China Commun.*, vol. 18, no. 5, pp. 93–119, May 2021.

[22] H. Lu, Y. Zeng, S. Jin, and R. Zhang, "Aerial intelligent reflecting surface: Joint placement and passive beamforming design with 3D beam flattening," *IEEE Trans. Wireless Commun.*, vol. 20, no. 7, pp. 4128–4143, Jul. 2021.

[23] F. Zhou, C. You, and R. Zhang, "Delay-optimal scheduling for IRS-aided mobile edge computing," *IEEE Wireless Commun. Lett.*, vol. 10, no. 4, pp. 740–744, Dec. 2021.

[24] W. Zhao, G. Wang, S. Atapattu, T. A. Tsiftsis, and X. Ma, "Performance analysis of large intelligent surface aided backscatter communication systems," *IEEE Wireless Commun. Lett.*, vol. 9, no. 7, pp. 962–966, Jul. 2020.

[25] S. Abeywickrama, C. You, R. Zhang, and C. Yuen, "Channel estimation for intelligent reflecting surface assisted backscatter communication," 2021, *arXiv:2103.08836*.

[26] X. Jia, X. Zhou, D. Niyato, and J. Zhao, "Intelligent reflecting surface-assisted bistatic backscatter networks: Joint beamforming and reflection design," 2020, *arXiv:2010.08947*.

[27] M. Nemati, J. Ding, and J. Choi, "Short-range ambient backscatter communication using reconfigurable intelligent surfaces," in *Proc. IEEE Wireless Commun. Netw. Conf. (WCNC)*, May 2020, pp. 1–6.

[28] Y.-C. Liang, Q. Zhang, E. G. Larsson, and G. Y. Li, "Symbiotic radio: Cognitive backscattering communications for future wireless networks," *IEEE Trans. Cognit. Commun. Netw.*, vol. 6, no. 4, pp. 1242–1255, Dec. 2020.

[29] X. Jia and X. Zhou, "IRS-assisted ambient backscatter communications utilizing deep reinforcement learning," 2021, *arXiv:2103.07083*.

[30] R. Fara, D.-T. Phan-Huy, P. Ratajczak, A. Ourir, M. Di Renzo, and J. de Rosny, "Reconfigurable intelligent surface-assisted ambient backscatter communications—Experimental assessment," 2021, *arXiv:2103.08427*.

[31] R. Fara, P. Ratajczak, D.-T. P. Huy, A. Ourir, M. D. Renzo, and J. D. Rosny, "A prototype of reconfigurable intelligent surface with continuous control of the reflection phase," 2021.

[32] H. Zheng, Z. Yang, G. Wang, R. He, and B. Ai, "Channel estimation for ambient backscatter communications with large intelligent surface," in *Proc. 11th Int. Conf. Wireless Commun. Signal Process. (WCSP)*, Oct. 2019, pp. 1–5.
[33] Q. Wu and R. Zhang, "Intelligent reflecting surface enhanced wireless network via joint active and passive beamforming," *IEEE Trans. Wireless Commun.*, vol. 18, no. 11, pp. 5394–5409, Nov. 2019.
[34] B. Zheng, C. You, W. Mei, and R. Zhang, "A survey on channel estimation and practical passive beamforming design for intelligent reflecting surface aided wireless communications," *IEEE Commun. Surveys Tuts.*, vol. 24, no. 2, pp. 1035–1071, Feb. 2022.
[35] D. M. Dobkin, *The RF in RFID: UHF RFID in Practice*. London, U.K.: Newnes, 2012.
[36] Y. Zhang, F. Gao, L. Fan, X. Lei, and G. K. Karagiannidis, "Backscatter communications over correlated Nakagami-*m* fading channels," *IEEE Trans. Commun.*, vol. 67, no. 2, pp. 1693–1704, Feb. 2019.
[37] M. Simon and M. Alouini, "*Digital Communication Over Fading Channels: A Unified Approach to Performance Analysis*. New York, NY, USA: Wiley, 2000.
[38] X. Lu, H. Jiang, D. Niyato, D. I. Kim, and Z. Han, "Wireless-powered device-to-device communications with ambient backscattering: Performance modeling and analysis," *IEEE Trans. Wireless Commun.*, vol. 17, no. 3, pp. 1528–1544, Mar. 2018.
[39] M. Vestakis, P. N. Alevizos, G. Vougioukas, and A. Bletsas, "Multistatic narrowband localization in backscatter sensor networks," in *Proc. IEEE 19th Int. Workshop Signal Process. Adv. Wireless Commun. (SPAWC)*, Jun. 2018, pp. 1–5.
[40] Y. Cheng, K. H. Li, Y. Liu, K. C. Teh, and H. V. Poor, "Downlink and uplink intelligent reflecting surface aided networks: NOMA and OMA," *IEEE Trans. Wireless Commun.*, vol. 20, no. 6, pp. 3988–4000, Jun. 2021.
[41] G. Wang, F. Gao, R. Fan, and C. Tellambura, "Ambient backscatter communication systems: Detection and performance analysis," *IEEE Trans. Commun.*, vol. 64, no. 11, pp. 4836–4846, Nov. 2016.
[42] Z.-Q. Luo and S. Zhang, "A semidefinite relaxation scheme for multivariate quartic polynomial optimization with quadratic constraints," *SIAM J. Optim.*, vol. 20, no. 4, pp. 1716–1736, Jan. 2010.
[43] Y. Sun, P. Babu, and D. Palomar, "Majorization-minimization algorithms in signal processing, communications, and machine learning," *IEEE Trans. Signal Process.*, vol. 65, no. 3, pp. 794–816, Feb. 2017.
[44] M. Grant and S. Boyd. (2016). *CVX: MATLAB Software for Disciplined Convex Programming*. [Online]. Available: http://cvxr.com/cvx
[45] N. D. Sidiropoulos, T. N. Davidson, and Z.-Q. Luo, "Transmit beamforming for physical-layer multicasting," *IEEE Trans. Signal Process.*, vol. 54, no. 6, pp. 2239–2251, Jun. 2006.
[46] X. Yu, D. Xu, and R. Schober, "MISO wireless communication systems via intelligent reflecting surfaces," in *Proc. IEEE/CIC Int. Conf. Commun. China (ICCC)*, Aug. 2019, pp. 735–740.
[47] C. Pan, H. Ren, K. Wang, W. Xu, M. Elkashlan, A. Nallanathan, and L. Hanzo, "Multicell MIMO communications relying on intelligent reflecting surfaces," *IEEE Trans. Wireless Commun.*, vol. 19, no. 8, pp. 5218–5233, May 2020.
[48] J. Qian, F. Gao, G. Wang, S. Jin, and H. Zhu, "Semi-coherent detection and performance analysis for ambient backscatter system," *IEEE Trans. Commun.*, vol. 65, no. 12, pp. 5266–5279, Dec. 2017.

SAHAR IDREES (Graduate Student Member, IEEE) received the B.S. degree in electrical engineering from the University of Engineering & Technology (UET) Lahore, Lahore, Pakistan, in 2007, and the M.S. degree in electrical engineering (communication theory and systems) from the University of California at San Diego, San Diego, USA, in 2009. She is currently pursuing the Ph.D. degree in electrical engineering with Australian National University (ANU), Canberra, Australia. She has been with the Department of Electrical Engineering, UET Lahore, since 2009, where she is currently on study leave. Her research interests include backscatter communication, energy harvesting, intelligent reflecting surfaces, and machine learning for wireless communication systems.

XIAOLUN JIA (Graduate Student Member, IEEE) received the B.E. degree in electronic and communication systems from Australian National University (ANU), in 2017, where he is currently pursuing the Ph.D. degree in communications engineering. His research interests include backscatter communication, intelligent reflecting surfaces, and performance analysis of wireless communication systems.

SALMAN DURRANI (Senior Member, IEEE) received the B.Sc. degree (Hons.) in electrical engineering from the University of Engineering & Technology Lahore, Lahore, Pakistan, in 2000, and the Ph.D. degree in electrical engineering from The University of Queensland, Brisbane, Australia, in December 2004.

He has been with Australian National University, Canberra, Australia, since 2005, where he is currently an Associate Professor with the Research School of Electrical, Energy and Materials Engineering, and the College of Engineering & Computer Science. His research interests include wireless information and power transfer, energy-harvesting-enabled wireless communications, drone communications, machine-to-machine and device-to-device communication, stochastic geometry modeling of finite area networks, and synchronization in communication systems. He has coauthored more than 150 publications to date in refereed international journals and conferences. He is a member of Engineers Australia and a Senior Fellow of The Higher Education Academy, U.K. He has been awarded multiple prizes, honours and awards for research, supervision, teaching, and service. He was a recipient of the 2016 IEEE ComSoc Asia Pacific Outstanding Paper Award. He was awarded the Special Commendation in the 2019 Australian Council of Graduate Research Award (ACGR) for Excellence in Graduate Research Supervision, 2018 ANU VC Award for Excellence in Supervision, and the 2012 ANU VC Award for Excellence in Education. He was awarded a Certificate of Appreciation for Notable Services and Contributions toward the advancement of Institute of Electrical & Electronics Engineers (IEEE) and the Engineering Profession, in 2018. He was the Chair of the ACT Chapter of the IEEE Signal Processing and Communications Societies, from 2015 to 2016. He currently serves as an Editor of the IEEE TRANSACTIONS ON COMMUNICATIONS.

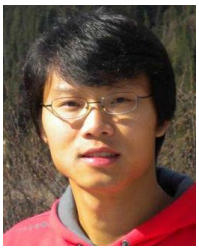

XIANGYUN ZHOU (Senior Member, IEEE) received the Ph.D. degree from Australian National University (ANU), in 2010. He is currently an Associate Professor with ANU. His research interests include the fields of communication theory and wireless networks. He has served as an Editor for various IEEE journals, including IEEE TRANSACTIONS ON WIRELESS COMMUNICATIONS, IEEE WIRELESS COMMUNICATIONS LETTERS, and IEEE COMMUNICATIONS LETTERS. He served as a Guest Editor for *IEEE Communications Magazine* feature topic on wireless physical layer security in 2015. He also served as a symposium/a track and workshop co-chairs for major IEEE conferences. He was the Chair of the ACT Chapter of the IEEE Communications Society and Signal Processing Society, from 2013 to 2014. He was a recipient of the Best Paper Award at ICC'11 and IEEE ComSoc Asia-Pacific Outstanding Paper Award, in 2016. He was named the Best Young Researcher in the Asia-Pacific Region, in 2017, by IEEE ComSoc Asia-Pacific Board.